SWEET-Cat update and FASMA

A new minimization procedure for stellar parameters using high-quality spectra[*],[**]

D. T. Andreasen[1,2], S. G. Sousa[1], M. Tsantaki[3], G.D.C. Teixeira[1,2], A. Mortier[4], N. C. Santos[1,2], L. Suárez-Andrés[5,6], E. Delgado-Mena[1], and A. C. S. Ferreira[1,2]

[1] Instituto de Astrofísica e Ciências do Espaço, Universidade do Porto, CAUP, Rua das Estrelas, 4150-762 Porto, Portugal e-mail: `daniel.andreasen@astro.up.pt`
[2] Departamento de Física e Astronomia, Faculdade de Ciências, Universidade do Porto, Rua Campo Alegre, 4169-007 Porto, Portugal
[3] Instituto de Radioastronomía y Astrofísica, IRyA, UNAM, Campus Morelia, A.P. 3-72, 58089 Michoacán, Mexico
[4] Centre for Exoplanet Science, SUPA, School of Physics and Astronomy, University of St Andrews, St Andrews KY16 9SS, UK- SUPA, School of Physics and Astronomy, University of St Andrews, St Andrews KY16 9SS, UK
[5] Depto. Astrofísica, Universidad de La Laguna (ULL), E-38206 La Laguna, Tenerife, Spain
[6] Instituto de Astrofísica de Canarias, E-38205 La Laguna, Tenerife, Spain

ABSTRACT

Context. Thanks to the importance that the star-planet relation has to our understanding of the planet formation process, the precise determination of stellar parameters for the ever increasing number of discovered extrasolar planets is of great relevance. Furthermore, precise stellar parameters are needed to fully characterize the planet properties. It is thus important to continue the efforts to determine, in the most uniform way possible, the parameters for stars with planets as new discoveries are announced.
Aims. In this paper we present new precise atmospheric parameters for a sample of 50 stars with planets. The results are presented in the catalogue: SWEET-Cat.
Methods. Stellar atmospheric parameters and masses for the 50 stars were derived assuming local thermodynamic equilibrium (LTE) and using high-resolution and high signal-to-noise spectra. The methodology used is based on the measurement of equivalent widths with ARES2 for a list of iron lines. The line abundances were derived using MOOG. We then used the curve of growth analysis to determine the parameters. We implemented a new minimization procedure which significantly improves the computational time.
Results. The stellar parameters for the 50 stars are presented and compared with previously determined literature values. For SWEET-Cat, we compile values for the effective temperature, surface gravity, metallicity, and stellar mass for almost all the planet host stars listed in the Extrasolar Planets Encyclopaedia. This data will be updated on a continuous basis. The data can be used for statistical studies of the star-planet correlation, and for the derivation of consistent properties for known planets.

Key words. planetary systems – stars: solar-type – catalogs

1. Introduction

The study of extrasolar planetary systems is an established field of research. To date, more than 3500 extrasolar planets have been discovered around more than 2500 solar-type stars[1]. Most of these planets have been found thanks to the incredible precision achieved in photometric transit and radial velocity methods. Not only do we have intriguing new types of planetary systems that challenge current theories, but the increasing number of exoplanets also allows us to do statistical studies of the newfound worlds by analysing their atmospheric composition, internal structure, and planetary composition.

Precise and accurate planetary parameters (mass, radius, and mean density) are needed to distinguish between solid rocky, water rich, gaseous, or otherwise composed planets. A key aspect to this progress is the characterization of the planet host stars. For instance, precise and accurate stellar radii are critical if we want to measure precise and accurate values of the radius of a transiting planet (see e.g. Torres et al. 2012; Mortier et al. 2013). The determination of the stellar radius is in turn dependent on the quality of the derived stellar atmospheric parameters such as the effective temperature.

We continue the work of Santos et al. (2013) by deriving atmospheric parameters, namely the effective temperature ($T_{\rm eff}$), surface gravity ($\log g$), metallicity ([Fe/H], where iron often is used as a proxy for the total metallicity), and the micro turbulence ($\xi_{\rm micro}$) for a sample of planet host stars. This, in turn, allows us to study new correlations between planets and their hosts in a homogeneous way or to gain higher statistical certainty on the already discovered correlations.

The analysis of high-quality spectra, i.e. spectra with high spectral resolution and a high signal-to-noise ratio (S/N), plays an important role in the derivation of stellar atmospheric parameters. Nevertheless, spectral analysis is a time consuming

---

method. There has been an increase in the number of optical high-resolution spectrographs available and, additionally, a number of near-IR spectrographs are either planned or are already available making the task of analysing the increasing amount of spectra even more crucial.

In the era of large data sets, computation time has to be decreased as much as possible without compromising the quality of the results. In the light of this we have developed a tool, FASMA, for deriving atmospheric parameters in a fast and robust way using standard spectroscopic methods. We made this tool available as a web interface[2]. This works well for optical spectra, which we demonstrate in Section 2.4 using the line list from Sousa et al. (2008) and Tsantaki et al. (2013). This tool also ships with a line list for near-IR spectra using the line list presented recently in Andreasen et al. (2016). The tool is provided to the community as an easy to use web tool to avoid any problems with installations. The tool is described in detail in Section 2. In Section 3.2 we present the new parameters for SWEET-Cat.

2. FASMA

Fast Analysis of Spectra Made Automatically (FASMA) is a web tool[3] for analysing spectra. FASMA is written in Python and works as a wrapper around ARES2 (Sousa et al. 2015) (hereafter just ARES) and MOOG (Sneden 1973, version 2014), for an all-in-one tool. ARES is a tool used to automatically measure equivalent widths (EW) from a spectrum given a line list. MOOG is a radiative transfer code under the assumption of local thermodynamic equilibrium (LTE).

FASMA has three different drivers: i) measuring EWs using ARES, ii) deriving stellar parameters from a set of measured Fe I and Fe II line EWs (tested extensively on FGK dwarf and subgiant stars), and iii) deriving abundances for 15 elements, all described below. The model atmospheres are formatted in a grid of Kurucz Atlas 9 plane-parallel, 1D static model atmospheres (Kurucz 1993). FASMA can also manage the new grid of Atlas models calculated by Mészáros et al. (2012) for the APOGEE survey and the MARCS models (Gustafsson et al. 2008). The interpolation from the grid is calculated from a geometric mean for effective temperature, surface gravity, and metallicity.

We do not consider hyper-fine structure (HFS) when deriving abundances since it has little or no effect on the derivation of iron abundances, so the derived parameters are trustworthy. If necessary, we might implement this in the future for elements where HFS is important.

2.1. Equivalent width measurements

The EWs are strongly correlated with the atmospheric parameters. Measurements of the EW can be done manually using a tool like splot in IRAF, but often when dealing with a large sample of stars this is not a suitable way to deal with the task. Therefore, there are several tools like ARES which can measure the EWs of spectral lines automatically. To use this mode of FASMA, a line list[4] and a spectrum (the format should be 1D fits for ARES to read it) are needed. FASMA is shipped with some line lists ready to use. The output will be a line list with the newly measured EWs in the format required for MOOG. The output can

---

[2] `http://www.iastro.pt/fasma`
[3] `http://www.iastro.pt/fasma`
[4] ARES, in principle, just needs a list of wavelengths in order to run, but is often used with a line list with characteristics of the atomic absorption line.

be used for either stellar parameter derivation or the abundance method, both described below. ARES iterates over all the lines to be measured. For each line a small window is selected, where a local normalization of the spectrum is made automatically. The normalization is made based on a range of settings described in Sousa et al. (2007, 2015). All of these settings can be changed in the driver. Most important is the *rejt* parameter, which we recommend measuring using the S/N of the spectrum. We note that for late K dwarfs and cooler, ARES starts to have difficulties placing the continuum. If the user wants EWs that are as accurate as possible, we recommend measuring by hand for these stars. The *rejt* parameter is a number between 0 and 1. When the value is closer to 1, which means higher quality of the spectrum, the normalization will use the higher points in the spectrum. By using the S/N, the *rejt* is simply, $rejt = 1 - 1/S/N$.

The line lists shipped with FASMA are presented in Table 1. These line lists are all calibrated for the Sun, i.e. the oscillator strengths for each absorption line are changed so the line with the measured EW from a solar spectrum return solar abundance for the given element.

Table 1. Line lists provided with FASMA. The first three line lists are for parameter determination while the last line list is used to derive abundances for 15 different elements.

Line list	Fe I/Fe II	Elements	Usage
Sousa et al. (2008)	263/36	1	Parameters
Tsantaki et al. (2013)	120/17	1	Parameters
Andreasen et al. (2016)	249/5	1	Parameters
Neves et al. (2009)	-/-	15	Abundances

2.2. Stellar parameter derivation

The standard determination of spectroscopic parameters for solar-type stars starts by measuring the EW of selected and well-defined absorption lines. Then we translate these measurements into individual line abundances, assuming a given atmospheric model. We obtain the correct stellar parameters by imposing excitation and ionization balance for the iron species. This is a classical curve-of-growth analysis using the Boltzmann and Saha equations,

$$\frac{N_n}{N} = \frac{g_n}{u(T)} 10^{-\theta \chi_n} \qquad \text{Boltzmann}$$

$$\frac{N_1}{N_0} P_e = \frac{(2\pi m_e)^{3/2}(kT)^{5/2}}{h^3} \frac{2u_1(T)}{u_0(T)} e^{-I/kT}, \qquad \text{Saha}$$

where N is the number of particles per unit volume, N_n is the fraction of atoms/ions excited to the nth state, g_n is the statistical weight, $\theta = 5040/T$, T is the temperature, $u(T)$ are the so-called partition functions, m_e is the electron mass, P_e is the electron pressure, and I is the ionization potential. More details can be found in e.g. Gray (2005). We note that the abundance determination are calculated through the MOOG code:

– The effective temperature has a strong influence on the correlation of iron abundance with the excitation potential (excitation balance). We obtain the T_{eff} when Fe I abundance shows no dependence on the excitation potential, i.e. the slope of abundance versus excitation potential is zero.
– Surface gravity is derived from the ionization balance of Fe I and Fe II abundances. Therefore, the abundance of neutral iron should be equal to the abundance of ionized iron and consistent with that of the input model atmosphere.
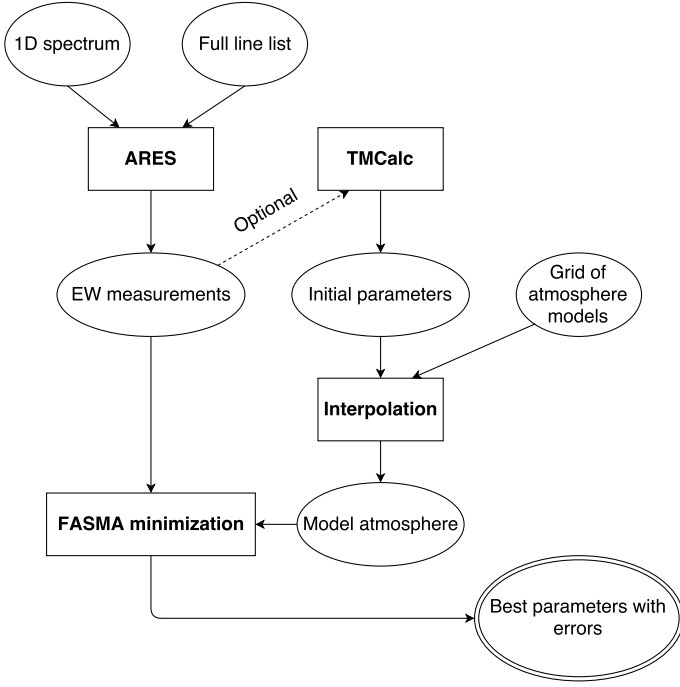
Fig. 1. General overview of FASMA from spectrum to parameters.

– Microturbulence is connected with the saturation of the stronger iron lines. However, the abundances for weak and strong lines of a certain species (in our case iron) should be the same independent of the value of ξ_{micro}. Iron abundances should show no dependence on the reduced EW $(\log(EW/\lambda))$, i.e. the slope of abundance versus the reduced EW is zero.

Lastly, we change the input [Fe /H] to match that of the average output [Fe /H]. Hence we have four criteria to minimize simultaneously:

1. The slope between abundance and excitation potential (a_{EP}) has to be lower than 0.001.
2. The slope between abundance and reduced EW (a_{RW}) has to be lower than 0.003. We use 0.003 rather than 0.001 since this slope varies more rapidly with small changes in atmospheric parameters.
3. The difference between the average abundances of Fe I and Fe II (ΔFe) should be less than 0.01.
4. Input and output metallicity should be equal.

These criteria are used as indicators for the physical parameters we are trying to minimize. The constraints on the first three indicators are empirically defined.

There are many minimization routines available in Python. The ones from the SciPy ecosystem[5] are the most commonly used. There are some advantages and disadvantages to using proprietary minimization routines. The advantages are that it is already written, and there is usually good documentation for libraries such as SciPy. The disadvantage in this situation is that most minimization routines do not work well with vector functions returning another vector:

$$f(\{T_{\mathrm{eff}}, \log g, [Fe/H], \xi_{\mathrm{micro}}\}) = \{a_{\mathrm{EP}}, a_{\mathrm{RW}}, \Delta\mathrm{Fe}, \mathrm{Fe\,I}\}. \qquad (1)$$

---
[5] http://scipy.org

A workaround to this is to combine the criteria into one single criterion, for example by adding them quadratically and minimizing that expression instead. Thus, we have a vector function returning a scalar:

$$f(\{T_{\mathrm{eff}}, \log g, [Fe/H], \xi_{\mathrm{micro}}\}) = \sqrt{a_{\mathrm{EP}}^2 + a_{\mathrm{RW}}^2 + \Delta\mathrm{Fe}^2}. \qquad (2)$$

The minimization routines are also not physical in the sense that they are not written for the problem. These two disadvantages encouraged us to write a specific minimization routine for the problem at hand. This also allowed us to minimize the more complicated expression in Equation 1. Here is how it works:

1. Run MOOG once with user defined initial parameters (default is solar) and calculate a_{EP}, a_{RW}, and $\Delta\mathrm{Fe}$.
2. Change the atmospheric parameters (T_{eff}, $\log g$, [Fe/H], ξ_{micro}) according to the size of the indicator. A parameter is only changed if it is not fixed.
   - a_{EP}: Indicator for T_{eff}. If this value is positive, then increase T_{eff}. Decrease T_{eff} if a_{EP} is negative.
   - a_{RW}: Same as above, but for ξ_{micro}.
   - $\Delta\mathrm{Fe}$: Positive $\Delta\mathrm{Fe}$ means $\log g$ should be decreased and vice versa.
   - [Fe /H] is changed to the output [Fe /H] in each iteration.
3. If the new set of parameters have already been used in a previous iteration, then change them slightly. This is done by drawing a random number from a Gaussian distribution with a mean at the current value and a sigma equal to the absolute value of the indicator. For T_{eff} the new value would be a random draw from $f(x|T_{\mathrm{eff,old}}, a_{\mathrm{EP}}^2) = \frac{1}{\sqrt{2\pi a_{\mathrm{EP}}^2}} e^{-\frac{(x-T_{\mathrm{eff,old}})^2}{2a_{\mathrm{EP}}^2}}$ and similar for the other atmospheric parameters using the appropriate indicators.
4. Calculate a new atmospheric model by interpolating a grid of models so we have the requested parameters and run MOOG once again.
5. For each iteration save the parameters used and the quadratic sum of the indicators.
6. Check for convergence, i.e. if the indicators are below or equal to the empirical constraints chosen. If we do not reach convergence, then return the best found parameters. The best found parameters, when convergence is not reached, are chosen when the quadratic sum of the indicators are smallest.

This whole process is shown schematically in Figure 1, and the minimization routine itself in Figure 2. By minimizing Equation 1 rather than Equation 2 we can reach convergence more quickly since we know in which direction we must change the atmospheric parameters. The stepping in parameters follows these simple empirical equations where we add the right side (sign change according to the sign of the indicator) to the left side:

$$T_{\mathrm{eff}} : 2000\,\mathrm{K} \cdot a_{\mathrm{EP}} \qquad (3)$$
$$\xi_{\mathrm{micro}} : 1.5\,\mathrm{km/s} \cdot a_{\mathrm{RW}} \qquad (4)$$
$$\log g : -\Delta\mathrm{Fe}. \qquad (5)$$

The metallicity is corrected at each step so the input metallicity matches that of the output metallicity of the previous iteration. The functional form (linear) for changing the parameters were found by changing one parameter, e.g. T_{eff}, while keeping the other parameters fixed at their convergence values using the Sun as an example. A linear fit was applied to $T_{\mathrm{eff}} - T_{\mathrm{eff,0}}$ versus a_{EP}
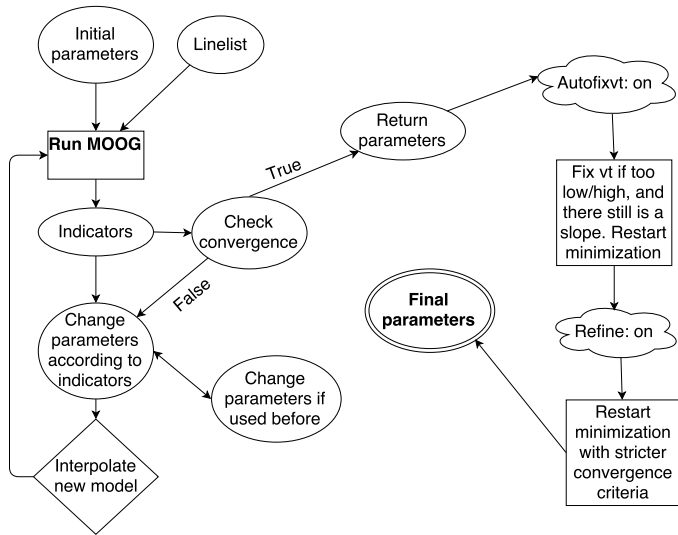
Fig. 2. Overview of the minimization for FASMA with the EW method.

in order to get the slope (2000 K for T_{eff}). Since we ignore all interdependencies between the parameters, we slightly lowered the slopes found and arrived at the very simple equations above. By empirically determining how the atmospheric parameters should be changed in each iteration, we are able to swiftly approach the convergence value. The error estimates are based on the same method presented in Gonzalez & Laws (2000), which is also described in detail in Santos et al. (2003) and Andreasen et al. (2016).

By using the indicators like this, we can reach convergence quickly. The typical calculation time for an FGK dwarf with a high-quality spectrum is around 2 min.

It is possible to run the EW method with a set of different options which are described here.

- *fixteff*: This option fixes T_{eff} and derives the other parameters. The same is available for $\log g$ (*fixlogg*), [Fe /H] (*fixfeh*), and ξ_{micro} (*fixvt*). One or more parameters can be fixed. When one or more parameters are fixed, the corresponding indicator will be ignored for each iteration, thus the parameter itself will not be changed.
- *outlier*: Remove a spectral line (or lines) after the the minimization is done if the abundance of this spectral line is more than 3σ away from the average abundance of all the lines. After the removal of outlier(s) the minimization routine restarts. The options are to remove all outliers above 3σ once or iteratively, or to remove one outlier above 3σ once or iteratively.
- *autofixvt*: If the minimization routine does not converge and ξ_{micro} is close to 0 or 10 with a significant a_{RW} (numerically bigger than 0.05), then fix ξ_{micro}. This option was added since we saw this behaviour in some cases. The solution was typically to restart the minimization manually with ξ_{micro} fixed. If ξ_{micro} is fixed it is changed at each iteration according to an empirical relation. For dwarfs it follows the one presented in Tsantaki et al. (2013) and for giants it follows the one presented in Adibekyan et al. (2015b).
- *refine*: After the minimization is done, run it again from the best found parameters but with stricter criteria. If this option is set, it will always be the last step (after removal of outliers). The convergence criteria can be changed by the user, but we recommend using the defaults provided above.
- *tmcalc*: Use TMCalc (Sousa et al. 2012) to quickly estimate the T_{eff} and [Fe /H] using the raw output from ARES. We

then assume solar surface gravity (4.44 dex) and estimate ξ_{micro} based on an empirical relation (see above).

For the optical we used the line list presented in Sousa et al. (2008). However, this line list does not work well for cool stars. This was fixed in Tsantaki et al. (2013) by removing some lines from Sousa et al. (2008). For stars cooler than 5200 K we automatically rederived the atmospheric parameters after removing lines so the line list resembled that of Tsantaki et al. (2013). The line list for the near-IR is also available (Andreasen et al. 2016).

All restarts of the minimization routine are done using the most recently found best parameters as initial conditions.

2.3. Abundance method

FASMA calculates element abundances for 12 different elements (Na , Mg , Al , Si , Ca , Ti , Cr , Ni , Co , Sc , Mn , and V) from spectral lines determined in Neves et al. (2009) and Adibekyan et al. (2012). It also includes three ionized elements: Cr ɪɪ, Sc 2, and Ti ɪɪ. The abundances are derived using MOOG in the same way as described above for Fe . The atomic data were calibrated with the Sun as reference and solar abundances from Anders & Grevesse (1989). The EWs are measured automatically with the ARES driver of FASMA. The element abundance of each line is derived using the atmospheric parameters of the stars obtained from the previous step. The final element abundance is calculated from the weighted mean of the abundances produced by all lines detected for a given element as described in Adibekyan et al. (2015a).

2.4. Testing FASMA

To test the derivation of stellar parameters implemented in FASMA we derived parameters from the 582 sample by Sousa et al. (2011). We used ARES to measure the EWs. ARES can give an estimate of the S/N by analysing the continuum in certain intervals. For solar-type stars the following intervals worked well: 5764-5766 Å, 6047-6053 Å, and 6068-6076 Å. From the estimated S/N, ARES can give an estimate on the very important *rejt* parameters (see Sousa et al. 2015, for more information). After measuring the EWs with ARES, we used the FASMA minimization routine described in Section 2.2 to determine the stellar atmospheric parameters. The results are presented in Figure 3 which shows T_{eff}, $\log g$, [Fe /H], and ξ_{micro} for FASMA against those of Sousa et al. (2011).

The sample contains stars with T_{eff} too cold for the line list used. As described in Section 2.2 we should then convert the line list by Sousa et al. (2008) to the line list presented in Tsantaki et al. (2013). However, since this line list was not available when Sousa et al. (2011) derived parameters, we did not make this change in order to make a fair comparison for FASMA.

The mean of the difference between parameters from Sousa et al. (2011) and those by FASMA are presented in Table 2.

The comparison is very consistent, as expected, and the small offsets are within the errors except for metallicity. This can be due to different versions of MOOG, measured line lists (i.e. using slightly different settings/version of ARES to measure the EWs), interpolation of atmosphere grid, and minimization routine. Most likely the difference will be due to the different *rejt* parameters used in ARES, which can alter the EWs systematically and hence the metallicity. We therefore randomly selected 20 stars with different T_{eff} and used the EWs directly from Sousa et al. (2011) to derive parameters. The results are presented in the last column of Table 2. We note that the $\log gf$ values from the
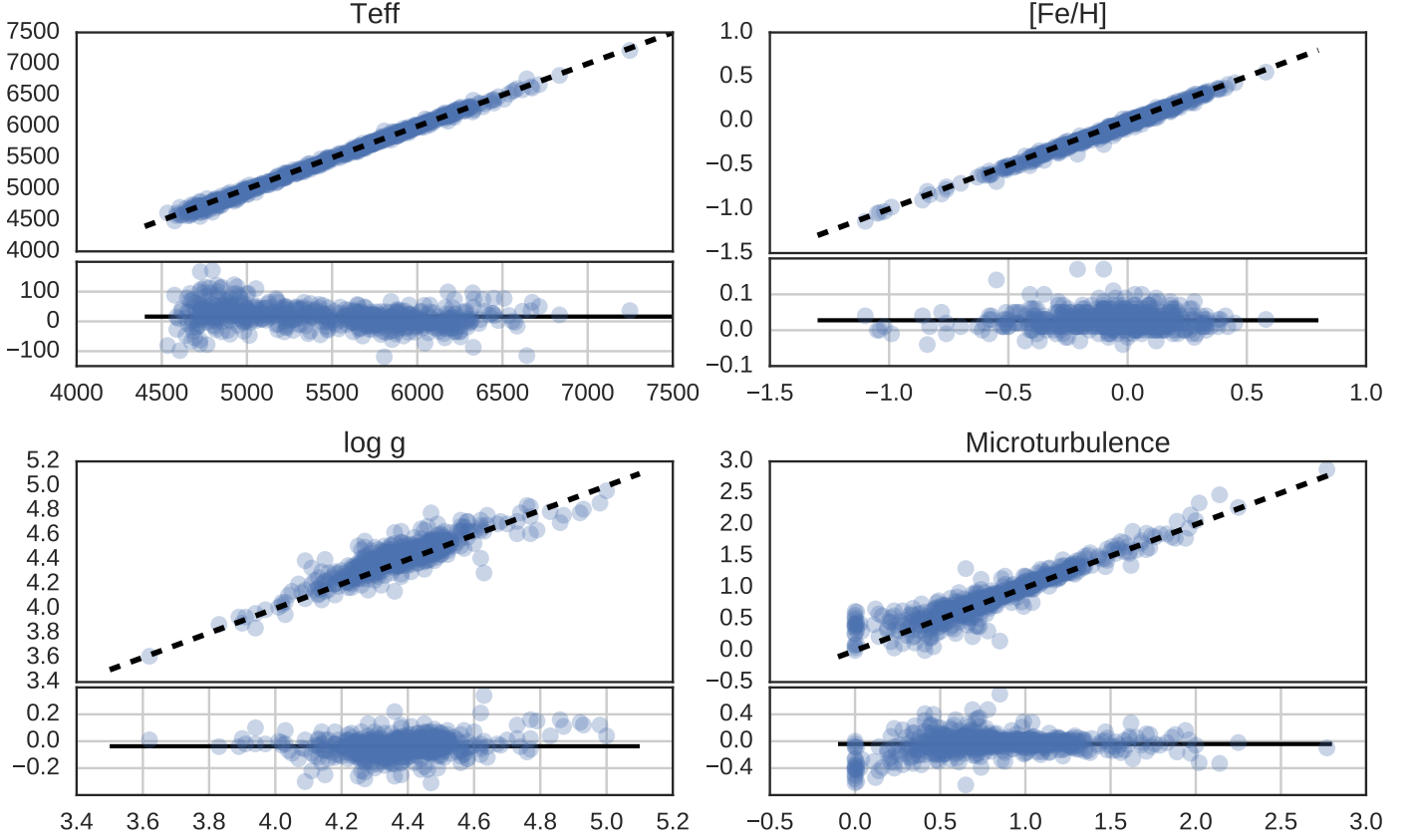
Fig. 3. Stellar atmospheric parameters derived by FASMA compared to the sample by Sousa et al. (2011). The x-axis in all plots shows the results from FASMA, while the y-axis shows the parameters derived by Sousa et al. (2011).

Table 2. Difference in derived parameters by Sousa et al. (2011) and FASMA. The second column is the mean difference with EWs measured by ARES in FASMA, while the third column is the mean difference using 20 randomly stars with the exact same EWs from Sousa et al. (2011).

Parameter	Mean difference	Same line list
T_{eff}	16 ± 36 K	21 ± 11 K
$\log g$	-0.04 ± 0.07	-0.007 ± 0.009
[Fe/H]	0.03 ± 0.02	0.004 ± 0.009
ξ_{micro}	-0.04 ± 0.14 km/s	0.04 ± 0.02 km/s

original line lists by Sousa et al. (2011), which used the MOOG 2002 version, were not changed for the 2014 version of MOOG. This might lead to some errors as well. However, the offsets are very small and are compatible with the errors on parameters normally obtained from high-quality spectra.

2.5. Web interface

We provide a web interface for FASMA. In the web interface it is possible to use the line list provided with FASMA to measure the EWs of a spectrum. The spectrum is expected to be in a 1D format with the wavelength information stored in the header keys, CRVAL1 for the minimum wavelength, CDELT1 for the stepping in wavelengths, and NAXIS1 for the number of points. This can be used for all the available FASMA methods described above. ARES does the normalization, but the best results are found when the spectrum is properly reduced (by removal of cosmic rays, normalization, etc.).

The web interface can be found at the following link `http://www.iastro.pt/fasma`, where more information is available on each of the drivers. The user must provide an email. This is only used to send the results after the calculations.

3. SWEET-Cat update

3.1. Data

In this paper we derived parameters for a sample of 50 stars, 43 were observed by our team using the UVES/VLT (Dekker et al. 2000), FEROS/2.2m telescope in La Silla (Kaufer et al. 1999), and FIES/NOT (Frandsen & Lindberg 1999) spectrographs. The remaining spectra (23) were found in various archives. We use spectra from the HARPS/3.6m telescope in La Silla (Mayor et al. 2003) and ESPaDOnS/CFHT (Donati 2003). Some characteristics of the spectrographs are presented in Table 3 with the mean S/N for the spectra used. The S/N for each star can be seen in Table A.1 along with the atmospheric parameters of the stars. The S/N is measured automatically by ARES, but we note that ARES smoothes the spectra before measuring the S/N, hence it is listed higher than the actual S/N. These 50 stars are confirmed exoplanet hosts listed in SWEET-Cat. However, they belonged

to the list of stars that have not been analysed by our team. We therefore increase the number of stars analysed in a homogeneous way, which is the goal of SWEET-Cat.

We obtain the spectra with the highest possible resolution for a given spectrograph, and in cases with multiple observations, we include all the observations unless a spectrum is close to the saturation limit for a given spectrograph. For multiple spectra, we combine them after first correcting the radial velocity (RV) and using a sigma clipper to remove cosmic rays. The individual spectra are then combined to a single spectrum for a given star to increase the S/N. This single spectrum is used in the analysis described below. For most of the spectra in the archive included here, several spectra were combined as described above, while for the observations dedicated to this work, the spectrum would be a single spectrum, or in cases of faint stars, it would be observed a few times to reach the desired S/N. This is mostly due to the difference in science cases behind the observations; for example, the HARPS spectra were used for RV monitoring or follow-up of the exoplanet(s), while the UVES spectra were used to characterize stellar parameters.

Table 3. Spectrographs used for this paper with their spectral resolution, wavelength coverage, and mean S/N from the spectra used.

Spectrograph	Resolution	Spectral range	Mean S/N
HARPS	115 000	378 − 691 nm	642
UVES	110 000	480 − 1100 nm	212
ESPaDOnS	81 000	370 − 1050 nm	775
FIES	67 000	370 − 730 nm	763
FEROS	48 000	350 − 920 nm	208

3.2. Analysis

Here we present the sample of 50 stars. We were unable to derive parameters for 16 of our targets (not included in the 50). For example, HD77065 is a spectroscopic binary according to Pourbaix et al. (2004), and the spectrum is contaminated by the companion star. This make EW measurement very difficult, hence we exclude it from the sample of collected spectra.

Moreover, we were not able to successfully derive parameters with this method for Aldebaran, a well-known red giant star. Even though spectra of good quality are available for a bright star like Aldebaran, this spectral type is intrinsically difficult to analyse, due to the molecular absorption that arises in the optical region at low $T_{\rm eff}$ (4055 K is listed in SWEET-Cat as measured by Hatzes et al. 2015). The fact that we are not able to derive parameters for Aldebaran is not a big concern since it has been well studied with other techniques, and we can trust the parameters already listed in SWEET-Cat.

In total, we removed 16 stars from our sample because the parameters for these stars did not converge during the minimization procedure. The $T_{\rm eff}$ for these stars is either too hot, above 7500 K, or too cold, below 4000 K, for the EW method to work.

The remaining 50 stars are presented in Table A.1. We note that we apply a correction to the spectroscopic $\log g$ based on asteroseismology as found by Mortier et al. (2014). We only use this correction for FGK dwarf stars, i.e. between 4800 K $\leq T_{\rm eff} \leq$ 6500 K and $\log g \geq 4.2$. For stars with a $\log g$ lower than this limit we do not apply the corrections, and if the $\log g$ changes to below this limit after the correction, we go back to using the spectroscopic $\log g$ again. The correction for $\log g$ depends on both $T_{\rm eff}$ and $\log g$. The correction can be up to 0.5 dex, depending on the $T_{\rm eff}$.
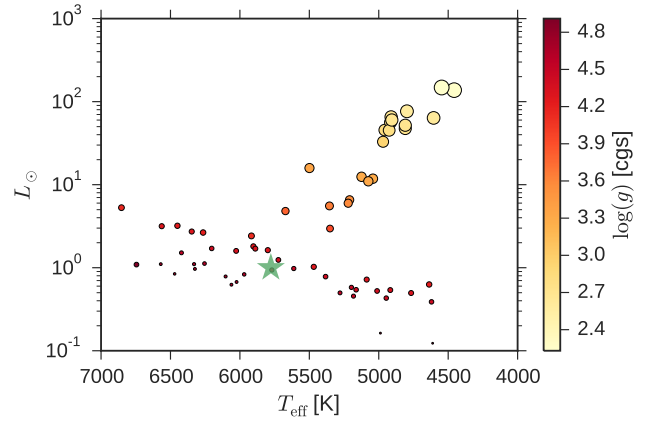
Fig. 4. Hertzsprung-Russel diagram of our sample with the Sun as a green star. The size of the points represents the $\log g$, with bigger points being smaller $\log g$ (giants), and vice versa. Red points are the dwarfs, while yellow points are the giants.

We present a Hertzsprung-Russel diagram (HRD) of our sample in Figure 4, which is made with a tool for post-processing the results saved to a table by FASMA.

The new atmospheric parameters are presented in Figure 5 against the literature values that we listed previously in SWEET-Cat. The red points showing the location of the outliers as discussed below are mainly visible outliers for $\log g$ at the low end, i.e. for the sub-giant to giant stars. The old parameters are listed in Table A.2. Out of 2437 stars discovered to be a planet hosts, 21% have been analysed in the homogeneous way as described in this work. We note that currently the limiting factor for increasing the sample of stars analysed in the homogeneous way is the magnitude of the planet hosts. Many planet hosts have been found through space missions such as *Kepler* and *CoRoT* using the transiting method. Most of these stars are faint and thus make them observationally expensive for the spectroscopic analysis required here. For stars brighter than magnitude 12 the completeness (i.e. the stars analysed in a homogeneous way compared to the ones we have not analysed yet) is now up to 77%, while it is at 85% for exoplanet hosts brighter than magnitude 10.

Understanding the metallicity distribution for all the planet host stars is important in order to understand planet formation, for example. We present a distribution in Figure 6. The sample is divided in two, for all planet hosts in SWEET-Cat and for stars brighter than 12 V magnitude. Dimmer stars are mainly observed with the *Kepler* space mission. These dim stars are very time consuming, and hence expensive to observe. Out of the 2437 stars in SWEET-Cat, 664 are brighter than 12 V magnitude. We note that more than 1500 of the stars do not have a V magnitude. The majority are stars observed with *Kepler*. Our group have analysed 563 stars in SWEET-Cat including the 50 stars presented in this work.

3.3. Discussion

We compute radius and mass of all the 50 new stars updated in SWEET-Cat (even the ones whose parameters may not be reliable, in order to be complete) using the empirical formula presented in Torres et al. (2010). Some of the stars have radii derived from different methods, usually from isochrones. These radii generally show a good correlation with radii derived from Torres et al. (2010) if the literature parameters of $T_{\rm eff}$, $\log g$, and
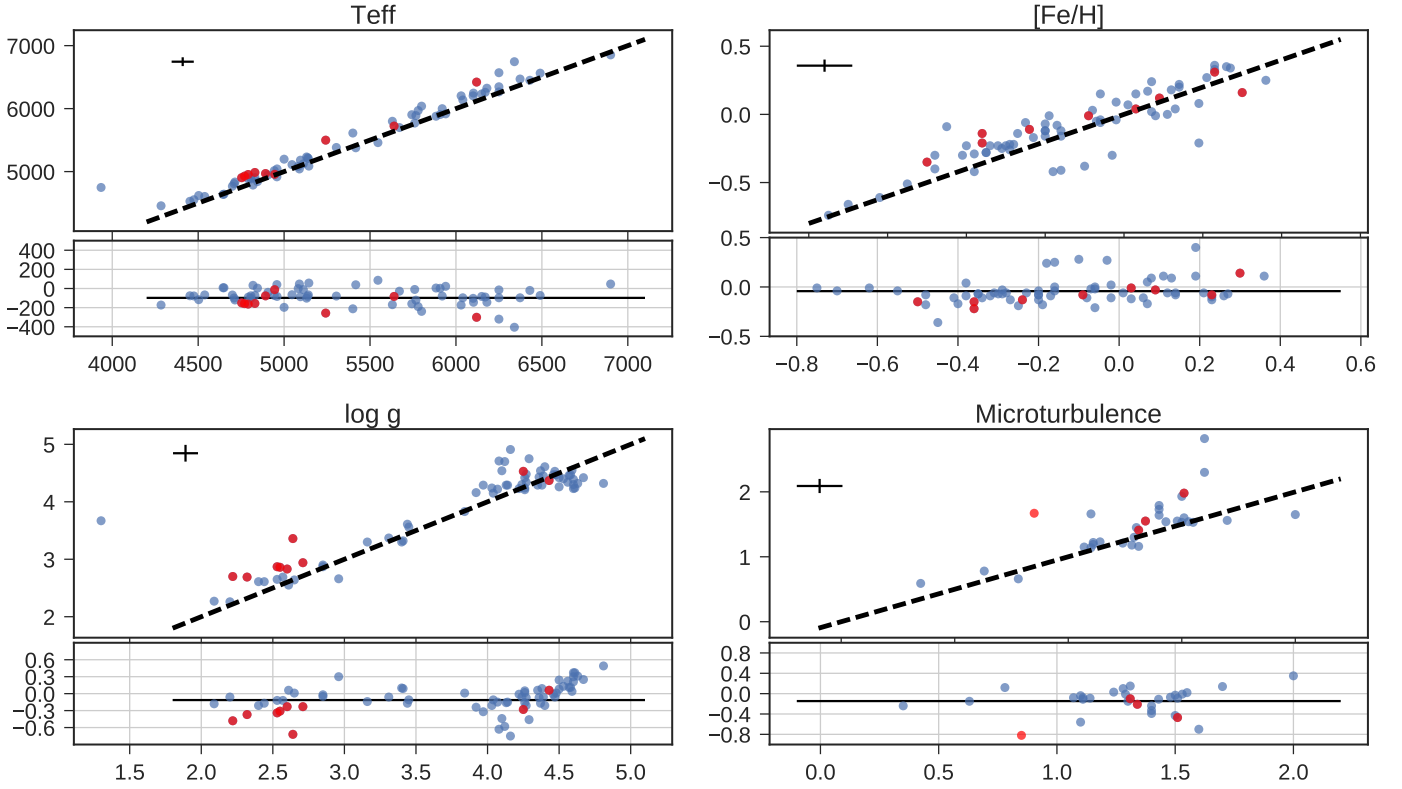
Fig. 5. Atmospheric parameters of the updated planet host stars. The x-axis shows the previous values in SWEET-Cat (see Table A.2), while the y-axis indicates the new updated values. In the upper left corner of each of the four plots we show the typical error on the parameters. The red points are outliers, as discussed in Section 3.3.
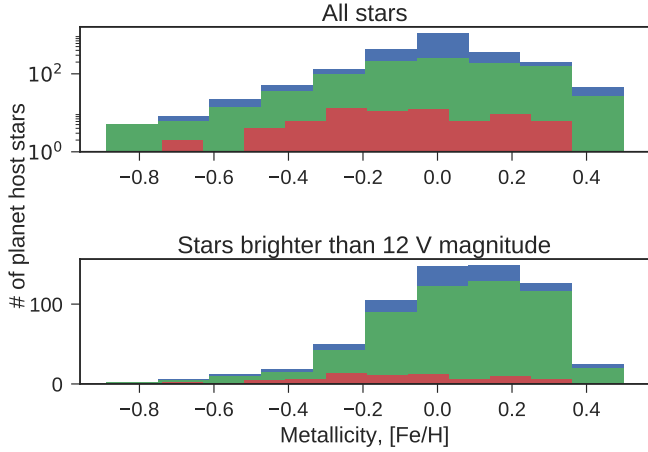

Fig. 6. Metallicity distribution. Top: All stars (logarithmic scale) in SWEET-Cat, divided in three groups: blue (the largest distribution) are all stars available in SWEET-Cat; green (the middle distribution) are the stars with homogeneity flag 1, i.e. analysed using the method described in this paper; and red (the smallest distribution) are all new stars added from this paper. Bottom: 12 V magnitude cut to exclude stars which are currently unavailable spectroscopically.

[Fe/H] are used. However, if we make a comparison with the new radius derived using the parameters presented here, the re-

sults can differ by up to 65%. We show in Figure 7 how the radius calculated from Torres et al. (2010) differs between the literature atmospheric parameters and the new homogeneous atmospheric parameters presented here. We note that stellar radii are provided by many of the authors from different discovery papers, but we chose to compare the atmospheric parameters via the derivation of the stellar radius, as described above, rather than comparing the stellar radii from different methods.

In the sections below we discuss the systems (seven stars, eight exoplanets) where the radius or mass of the stars changes more than 25% and how this influences the planetary parameters. The changes in radius for a star is primarily due to changes in $\log g$, which can be used as an indicator of the evolutionary stage of a star.

We rederive the planetary radius, mass, and semi-major axis when possible following the three simple scaling relations based on Newton's law of gravity (Newton 1687) for deriving mass and distance and simple geometry for radius (see e.g. Torres et al. 2008)
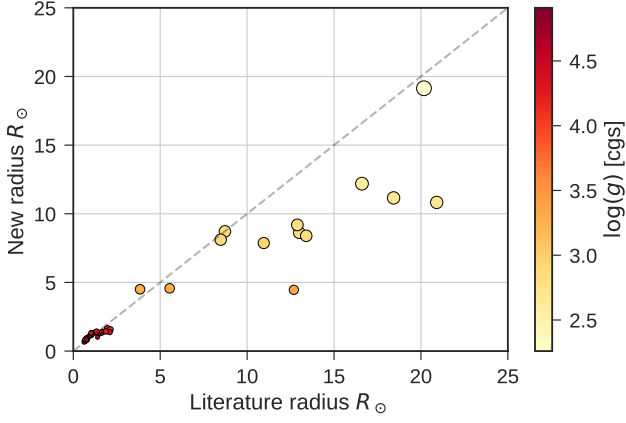
Fig. 7. Stellar radius on both axes calculated based on Torres et al. (2010). The x-axis shows the stellar radius based on the atmospheric parameters from the literature, while the y-axis indicates the new homogeneous parameters presented here. The colour and size indicate the surface gravity. This clearly shows that the disagreement is biggest for more evolved stars.

$$M_{\rm pl,new} = \left(\frac{M_{*,\rm lit}}{M_{*,\rm new}}\right)^{-2/3} M_{\rm pl,lit} \tag{6}$$

$$R_{\rm pl,new} = \left(\frac{R_{*,\rm lit}}{R_{*,\rm new}}\right) R_{\rm pl,lit} \tag{7}$$

$$a_{\rm pl,new} = \left(\frac{M_{*,\rm lit}}{M_{*,\rm new}}\right)^{1/3} a_{\rm pl,lit}, \tag{8}$$

where the subscript "lit" denotes the value from the literature used in the comparison, the subscript "new" indicates the new computed values, the subscript "pl" is short for planet, and the subscript "*" is short for star; M, R, and a are mass, radius, and semi-major axis, respectively. We note that for the literature values, we use the values reported directly from the literature and not the derived radius and mass from Torres et al. (2010). To identify outliers, we compare radii and masses derived from Torres et al. (2010) since this is a measure of how the atmospheric parameters have changed.

3.3.1. HAT-P-46

HAT-P-46 has two known exoplanets according to Hartman et al. (2014a). The outer planet HAT-P-46 c is not transiting, hence we do not have a radius for this planet. The results we present in this paper for this star come from UVES/VLT data with a S/N of 208. Hartman et al. (2014a) derives the following spectroscopic parameters: $T_{\rm eff} = 6120 \pm 100$ K, $\log g = 4.25 \pm 0.11$, and [Fe /H] $= 0.30 \pm 0.10$. We note that for this star the asteroseismic correction we apply (see Section 3.2) results in a corrected $\log g$ below 4.2dex, so we used the spectroscopic $\log g$ for this star.

If we derive the mass and radius of HAT-P-46 b with our new parameters, we obtain $R_{\rm pl} = 0.93R_J$, while Hartman et al. (2014a) derived $R_{\rm pl} = 1.28R_J$. We see no change in mass (Hartman et al. 2014a found $M_{\rm pl} = 0.49M_J$); however, there is a decrease in the radius, and we end up with a more dense planet, $\rho_{\rm pl} = 0.76$ g/cm^3 from $\rho_{\rm pl} = 0.28 \pm 0.10$ g/cm^3.

As the secondary companion does not transit we only have a limit on the minimum mass for this planet. Here we get

$M \sin i_{\rm pl} = 1.97M_J$ and Hartman et al. (2014a) presented $M \sin i_{\rm pl} = 2.00M_J$, so a very small change, as expected.

3.3.2. HD 120084

The exoplanet orbiting this star with a period of 2082 days and a quite eccentric orbit at 0.66 was discovered by Sato et al. (2013a). The atmospheric parameters were derived by Takeda et al. (2008) using a similar method to that described in this paper. The quality of the spectra they analysed, however, were not as high as those used here. Using the HIDES spectrograph at the 188cm reflector at NAOJ, Takeda et al. (2008) reported an average S/N for their sample of 100-300 objects at a resolving power of 67 000. We used data from ESPaDOnS with a resolving power of 81 000, and with a S/N for this star of 850. With our new parameters we obtain a slightly lower stellar mass for the star at $1.93M_\odot$ compared to $2.39M_\odot$ obtained by Takeda et al. (2008), hence the minimum planetary mass is also slightly lower, from $m_{\rm pl} \sin i = 4.5M_J$ to $m_{\rm pl} \sin i = 3.9M_J$. We see a 28% decrease in the stellar radius, from $9.12R_\odot$ to $7.81R_\odot$. Since there are no observations of the planet transiting, the planetary radius has not been computed.

3.3.3. HD 233604

HD 233604 b was discovered by Nowak et al. (2013), while the atmospheric parameters of the star were derived by Zieliński et al. (2012), who used the same method as described in this paper using the HRS spectrograph at HET with a resolving power of 60 000 with a typical S/N at 200-250. We obtained the spectrum for this star using the FIES spectrograph with a slightly higher resolution at 67 000, and similar but also slightly higher S/N at 320 for this star.

This planet is in a very close orbit with a semi-major axis of $\sim 15R_*$ (R_* is the stellar radius) using the parameters from Nowak et al. (2013). Using the updated parameters presented in this paper we see a slight increase in the stellar mass from $1.5M_\odot$ to $1.9M_\odot$, and a decrease in stellar radius from $10.5R_\odot$ to $8.6R_\odot$. This increases the semi-major axis to $\sim 21R_*$. We note that the correct stellar radii are used to describe the semi-major axis in both cases. The increase in stellar mass leads to an increase in the minimum planetary mass, from $m_{\rm pl} \sin i = 6.58M_J$ to $m_{\rm pl} \sin i = 7.79M_J$.

Nowak et al. (2013) found a high Li abundance at $A(\text{Li})_{\rm LTE} = 1.400 \pm 0.042$ for this star and speculated that this star might have engulfed a planet. A more likely explanation is that this star has not yet reached the first dredge-up process (Nowak et al. 2013). We found a much lower value, $A(\text{Li})_{\rm LTE} = 0.92$, and hence do not find the star to be Li rich. The Li abundance we find is in excellent agreement with Adamów et al. (2014). Even applying a NLTE correction, as was done in Adamów et al. (2014) ($A(\text{Li})_{\rm NLTE} = 1.08$), this star is not Li rich.

3.3.4. HD 5583

This exoplanet was discovered by Niedzielski et al. (2016) with an orbital period of 139 days around a K giant. This exoplanet was discovered with the radial velocity technique, and we do not have a planetary radius. The stellar parameters were derived in a similar manner to that presented here (see Niedzielski et al. 2016, and references therein); our biggest disagreement is in the surface gravity. We derive a $\log g$ that is higher by 0.34 dex, which gives a stellar radius that is smaller by 37%. The derived

mass is 15% higher, which in turn increases the minimum planetary mass from $m_{pl} \sin i = 5.78 M_J$ to $m_{pl} \sin i = 8.63 M_J$. Even with the increase in mass, it is still within the planetary regime for most inclinations, as was noted by Niedzielski et al. (2016).

3.3.5. HD 81688

This exoplanet was discovered by Sato et al. (2008) with the RV method. The host star is a metal-poor K giant. The atmospheric parameters presented in Sato et al. (2008) are obtained via the same method as presented in this paper, and the agreement is quite good. Once again the big disagreement is in the surface gravity: ours is 0.48 dex higher. Even though the stellar parameters, and hence the planetary parameters, do change, the radius and mass we derive are not far from the values presented in the paper by Sato et al. (2008). This is a case where the star was marked as an outlier, due to the comparison between the radius and mass derived from Torres et al. (2010).

The new stellar mass is the same as before, $2.1 M_\odot$. The stellar radius changed from $13.0 R_\odot$ to $10.8 R_\odot$. Since a transit of this star has not been observed and the stellar mass remains the same, we do not see any change in the planetary parameters.

We note that this system is in an interesting configuration with a very close orbit around an evolved star. This system, among others, has been the subject of work on planet engulfment (see e.g. Kunitomo et al. 2011).

3.3.6. HIP 107773

The planetary companion was presented in Jones et al. (2015) as an exoplanet around an intermediate-mass evolved star. The stellar parameters were obtained from the analysis by Jones et al. (2011) using the same method as presented here, but with a different line list, which might lead to some disagreements. For this star we derive a higher $\log g$ (2.83 dex compared to 2.60 dex), thus we derive a slightly smaller star with $11.6 R_\odot$ to $9.2 R_\odot$ and $2.4 M_\odot$ to $2.1 M_\odot$ for radius and mass of the star, respectively. The other atmospheric parameters are very similar to those derived by Jones et al. (2011). This leads to a reduced minimum mass of the planetary companion from $m \sin i = 1.98 M_J$ to $m \sin i = 1.78 M_J$. The planetary radius has not been measured.

3.3.7. WASP-97

The exoplanet orbiting WASP-97 was discovered by Hellier et al. (2014). The host star parameters were derived using a similar method to that described in this paper after co-adding several spectra from the CORALIE spectrograph. They reach a S/N of 100 with a spectral resolution of 50 000. The parameters presented here come from the UVES spectrograph with a S/N of more than 200.

The parameters do not change much for this planet. The planetary mass changes from $m_{pl} \sin i = 1.32 M_J$ to $m_{pl} \sin i = 1.37 M_J$ and the radius from $1.13 R_J$ to $1.42 R_J$. This affects the density quite strongly; it changes from $1.13 \, g/cm^3$ to $0.59 \, g/cm^3$. This exoplanet is then in the same category as Saturn; its density is lower than water, but it is slightly larger than Jupiter.

3.3.8. ω Serpentis (ome Ser)

The exoplanet orbiting this star with a period of 277 days and an eccentric orbit at 0.11 was also presented by Sato et al. (2013a).

The atmospheric parameters were derived in the same way as for HD 120084. We used data from FIES with a resolving power of 67 000, and with a S/N for this star of 1168. With our new parameters we obtain a slightly higher stellar mass for the star at $2.19 M_\odot$ compared to the value of $2.17 M_\odot$ obtained by Takeda et al. (2008). This change is not significant enough to change the minimum planetary mass at $m_{pl} \sin i = 1.7 M_J$. The stellar radius decreases by more than one solar radius, from $12.3 R_\odot$ to $11.1 R_\odot$. However, since there are no observations of transiting exoplanets, we cannot see the change in the planetary radius.

3.3.9. o Ursa Major (omi UMa)

omi UMa b was discovered by Sato et al. (2012) using the RV method. The stellar parameters are from Takeda et al. (2008), as discussed above. The spectrum used for this star is from ESPaDOnS with a S/N of more than 500 compared to the value of 100-300 reached for the large sample presented in Takeda et al. (2008). The luminosity and mass for omi UMa were obtained from theoretical evolutionary tracks (see Sato et al. 2012, and references therein). The radius was then estimated using the Stefan-Boltzmann relationship, using the measured luminosity and T_{eff}.

The parameters presented here mainly differ in the surface gravity: ours is 0.72 dex higher at $\log g = 3.36$. This leads to a big change in stellar mass and radius from $3.1 M_\odot$ to $1.6 M_\odot$ and $14.1 R_\odot$ to $4.5 R_\odot$, respectively. Sato et al. (2012) have reported that omi UMa b is the first planet candidate around a star more massive than $3 M_\odot$. With these updated results, the minimum mass of the planet is now $m \sin i = 2.7 M_J$, whereas previously it was $m \sin i = 4.1 M_J$ (Sato et al. 2012). The exoplanet is not reported to transit, as seen from Earth, so we do not have a radius for this exoplanet, which would have changed a great deal with these new results.

4. Conclusion

With this update we bring the completeness of SWEET-Cat for stars brighter than magnitude 10 (V band) up to 85% (77% for stars brighter than 12). The parameters are continuously updated and are available for the public in an easily accessibly form[6]. The importance of the homogeneous analysis which we keep striving for is shown in Figure 7 where we see quite different derived stellar radii when the atmospheric parameters are obtained via different methods. Even using the same method but with a different setup (different line list, minimization routine, atmospheric models, etc.), we can arrive at different results. This again shows the importance of analysing the stars in a homogeneous way. As has been discussed in Section 3.3 this has a direct impact on the planetary parameters. It is of great importance to know the planetary parameters very well, for individual systems and also for an ensemble. With accurate and precise planetary parameters we will be able to distinguish the different possible compositions, whether gas giants, water worlds, or rocky planets.

Finally we also provide an online tool for deriving the stellar atmospheric parameters using FASMA. We recommend this tool only for spectra and stars where this method is working, i.e. high-resolution spectra with a high S/N. The stars can be FGK dwarfs and FGK subgiants/giants. We are working on applying this method to the near-IR in order to include the cool solar-type stars.

---

[6] https://www.astro.up.pt/resources/sweet-cat/

References

Adamów, M., Niedzielski, A., Villaver, E., Wolszczan, A., & Nowak, G. 2014, A&A, 569, A55

Adibekyan, V., Figueira, P., Santos, N. C., et al. 2015a, A&A, 583, A94

Adibekyan, V. Z., Benamati, L., Santos, N. C., et al. 2015b, MNRAS, 450, 1900

Adibekyan, V. Z., Sousa, S. G., Santos, N. C., et al. 2012, A&A, 545, A32

Anders, E. & Grevesse, N. 1989, Geochim. Cosmochim. Acta, 53, 197

Anderson, D. R., Collier Cameron, A., Gillon, M., et al. 2012, MNRAS, 422, 1988

Andreasen, D. T., Sousa, S. G., Delgado Mena, E., et al. 2016, A&A, 585, A143

Barclay, T., Rowe, J. F., Lissauer, J. J., et al. 2013, Nature, 494, 452

Bedell, M., Meléndez, J., Bean, J. L., et al. 2015, A&A, 581, A34

Boisse, I., Hartman, J. D., Bakos, G. Á., et al. 2013, A&A, 558, A86

Brucalassi, A., Pasquini, L., Saglia, R., et al. 2014, A&A, 561, L9

Bryan, M. L., Alsubai, K. A., Latham, D. W., et al. 2012, ApJ, 750, 84

Campante, T. L., Barclay, T., Swift, J. J., et al. 2015, ApJ, 799, 170

Collins, K. A., Eastman, J. D., Beatty, T. G., et al. 2014, AJ, 147, 39

Dekker, H., D'Odorico, S., Kaufer, A., Delabre, B., & Kotzlowski, H. 2000, in Proc. SPIE, Vol. 4008, Optical and IR Telescope Instrumentation and Detectors, ed. M. Iye & A. F. Moorwood, 534–545

Delrez, L., Van Grootel, V., Anderson, D. R., et al. 2014, A&A, 563, A143

Donati, J.-F. 2003, in Astronomical Society of the Pacific Conference Series, Vol. 307, Solar Polarization, ed. J. Trujillo-Bueno & J. Sanchez Almeida, 41

Frandsen, S. & Lindberg, B. 1999, in Astrophysics with the NOT, ed. H. Karttunen & V. Piirola, 71

Gillon, M., Anderson, D. R., Collier-Cameron, A., et al. 2013, A&A, 552, A82

Gómez Maqueo Chew, Y., Faedi, F., Pollacco, D., et al. 2013, A&A, 559, A36

Gonzalez, G. & Laws, C. 2000, AJ, 119, 390

Gray, D. F. 2005, The Observation and Analysis of Stellar Photospheres, 3rd ed.

Gustafsson, B., Edvardsson, B., Eriksson, K., et al. 2008, A&A, 486, 951

Hartman, J. D., Bakos, G. Á., Béky, B., et al. 2012, AJ, 144, 139

Hartman, J. D., Bakos, G. Á., Torres, G., et al. 2014a, AJ, 147, 128

Hartman, J. D., Bakos, G. Á., Torres, G., et al. 2014b, AJ, 147, 128

Hatzes, A. P., Cochran, W. D., Endl, M., et al. 2015, A&A, 580, A31

Hébrard, G., Arnold, L., Forveille, T., et al. 2016, A&A, 588, A145

Hébrard, G., Collier Cameron, A., Brown, D. J. A., et al. 2013, A&A, 549, A134

Hellier, C., Anderson, D. R., Cameron, A. C., et al. 2014, MNRAS, 440, 1982

Hellier, C., Anderson, D. R., Collier Cameron, A., et al. 2012, MNRAS, 426, 739

Howard, A. W., Johnson, J. A., Marcy, G. W., et al. 2011, ApJ, 730, 10

Johnson, J. A., Clanton, C., Howard, A. W., et al. 2011, ApJS, 197, 26

Jones, M. I., Jenkins, J. S., Rojo, P., & Melo, C. H. F. 2011, A&A, 536, A71

Jones, M. I., Jenkins, J. S., Rojo, P., Olivares, F., & Melo, C. H. F. 2015, A&A, 580, A14

Kaufer, A., Stahl, O., Tubbesing, S., et al. 1999, The Messenger, 95, 8

Kipping, D. M., Bakos, G. Á., Hartman, J., et al. 2010, ApJ, 725, 2017

Kunitomo, M., Ikoma, M., Sato, B., Katsuta, Y., & Ida, S. 2011, ApJ, 737, 66

Kurucz, R. 1993, ATLAS9 Stellar Atmosphere Programs and 2 km/s grid. Kurucz CD-ROM No. 13. Cambridge, Mass.: Smithsonian Astrophysical Observatory, 1993., 13

Lee, B.-C., Han, I., & Park, M.-G. 2013, A&A, 549, A2

Lee, B.-C., Han, I., Park, M.-G., et al. 2014, A&A, 566, A67

Mayor, M., Pepe, F., Queloz, D., et al. 2003, The Messenger, 114, 20

Mészáros, S., Allende Prieto, C., Edvardsson, B., et al. 2012, AJ, 144, 120

Mortier, A., Santos, N. C., Sousa, S., et al. 2013, A&A, 551, A112

Mortier, A., Sousa, S. G., Adibekyan, V. Z., Brandão, I. M., & Santos, N. C. 2014, A&A, 572, A95

Motalebi, F., Udry, S., Gillon, M., et al. 2015, A&A, 584, A72

Moutou, C., Lo Curto, G., Mayor, M., et al. 2015, A&A, 576, A48

Neves, V., Santos, N. C., Sousa, S. G., Correia, A. C. M., & Israelian, G. 2009, A&A, 497, 563

Neveu-VanMalle, M., Queloz, D., Anderson, D. R., et al. 2014, A&A, 572, A49

Newton, I. 1687, Philosophiae Naturalis Principia Mathematica. Auctore Js. Newton

Niedzielski, A., Villaver, E., Nowak, G., et al. 2016, A&A, 588, A62

Niedzielski, A., Villaver, E., Wolszczan, A., et al. 2015a, A&A, 573, A36

Niedzielski, A., Wolszczan, A., Nowak, G., et al. 2015b, ApJ, 803, 1

Nowak, G., Niedzielski, A., Wolszczan, A., Adamów, M., & Maciejewski, G. 2013, ApJ, 770, 53

Penev, K., Bakos, G. Á., Bayliss, D., et al. 2013, AJ, 145, 5

Pourbaix, D., Tokovinin, A. A., Batten, A. H., et al. 2004, A&A, 424, 727

Quinn, S. N., White, R. J., Latham, D. W., et al. 2014, ApJ, 787, 27

Santos, N. C., Israelian, G., Mayor, M., Rebolo, R., & Udry, S. 2003, A&A, 398, 363

Santos, N. C., Sousa, S. G., Mortier, A., et al. 2013, A&A, 556, A150

Sato, B., Izumiura, H., Toyota, E., et al. 2008, PASJ, 60, 539

Sato, B., Omiya, M., Harakawa, H., et al. 2012, PASJ, 64 [e-prints[arXiv]1207.3141]

Sato, B., Omiya, M., Harakawa, H., et al. 2013a, PASJ, 65 [e-prints[arXiv]1304.4328]

Sato, B., Omiya, M., Wittenmyer, R. A., et al. 2013b, ApJ, 762, 9

Simpson, E. K., Faedi, F., Barros, S. C. C., et al. 2011, AJ, 141, 8

Sneden, C. A. 1973, PhD thesis, THE UNIVERSITY OF TEXAS AT AUSTIN.

Sousa, S. G., Santos, N. C., Adibekyan, V., Delgado-Mena, E., & Israelian, G. 2015, A&A, 577, A67

Sousa, S. G., Santos, N. C., & Israelian, G. 2012, A&A, 544, A122

Sousa, S. G., Santos, N. C., Israelian, G., Mayor, M., & Monteiro, M. J. P. F. G. 2007, A&A, 469, 783

Sousa, S. G., Santos, N. C., Israelian, G., Mayor, M., & Udry, S. 2011, A&A, 533, A141

Sousa, S. G., Santos, N. C., Mayor, M., et al. 2008, A&A, 487, 373

Takeda, Y., Sato, B., & Murata, D. 2008, PASJ, 60, 781

Torres, G., Andersen, J., & Giménez, A. 2010, A&A Rev., 18, 67

Torres, G., Fischer, D. A., Sozzetti, A., et al. 2012, ApJ, 757, 161

Torres, G., Winn, J. N., & Holman, M. J. 2008, ApJ, 677, 1324

Tsantaki, M., Sousa, S. G., Adibekyan, V. Z., et al. 2013, A&A, 555, A150

Valenti, J. A. & Fischer, D. A. 2005, ApJS, 159, 141

Vanderburg, A., Montet, B. T., Johnson, J. A., et al. 2015, ApJ, 800, 59

West, R. G., Hellier, C., Almenara, J.-M., et al. 2016, A&A, 585, A126

Wilson, P. A., Hébrard, G., Santos, N. C., et al. 2016, A&A, 588, A144

Zhou, G., Bayliss, D., Penev, K., et al. 2014, AJ, 147, 144

Zieliński, P., Niedzielski, A., Wolszczan, A., Adamów, M., & Nowak, G. 2012, A&A, 547, A91

Appendix A: Updated parameters of 50 planet hosts

Table A.1. Derived parameters for the 50 stars in our sample. The S/N was measured by ARES.

Star	T_{eff} (K)	$\log g$ (dex)	[Fe/H] (dex)	ξ_{micro} (km/s)	ξ_{micro} fixed?	Instrument	S/N
BD -11 4672	4553 ± 75	4.87 ± 0.51	-0.30 ± 0.02	0.14 ± 0.07	yes	FIES	487
BD +49 828	5015 ± 36	2.87 ± 0.09^a	-0.01 ± 0.03	1.48 ± 0.04	no	FIES	567
GJ 785	5087 ± 48	4.42 ± 0.10	-0.01 ± 0.03	0.69 ± 0.10	no	HARPS	801
HATS-1	5969 ± 46	4.39 ± 0.06	-0.04 ± 0.04	1.06 ± 0.08	no	UVES	155
HATS-5	5383 ± 91	4.41 ± 0.22	0.08 ± 0.06	0.91 ± 0.14	no	UVES	158
HAT-P-12	4642 ± 106	4.53 ± 0.27	-0.26 ± 0.06	0.28 ± 0.63	no	FIES	185
HAT-P-24	6470 ± 181	4.33 ± 0.27	-0.41 ± 0.10	1.40 ± 0.03	yes	UVES	158
HAT-P-39	6745 ± 236	4.39 ± 0.47	-0.21 ± 0.12	1.53 ± 0.04	yes	UVES	127
HAT-P-42	5903 ± 66	4.29 ± 0.10^a	0.34 ± 0.05	1.19 ± 0.08	no	UVES	130
HAT-P-46	6421 ± 121	4.53 ± 0.14^a	0.16 ± 0.09	1.67 ± 0.18	no	UVES	208
HD 120084	4969 ± 40	2.94 ± 0.14^a	0.12 ± 0.03	1.41 ± 0.04	no	ESPaDOnS	852
HD 192263	4946 ± 46	4.61 ± 0.14	-0.05 ± 0.02	0.66 ± 0.12	no	HARPS	415
HD 219134	4767 ± 70	4.57 ± 0.17	0.00 ± 0.04	0.59 ± 0.24	no	ESPaDOnS	725
HD 220842	5999 ± 39	4.30 ± 0.06^a	-0.08 ± 0.03	1.21 ± 0.05	no	FIES	459
HD 233604	4954 ± 46	2.86 ± 0.11^a	-0.14 ± 0.04	1.61 ± 0.05	no	FIES	314
HD 283668	4841 ± 73	4.51 ± 0.18	-0.74 ± 0.04	0.16 ± 0.61	no	FIES	592
HD 285507	4620 ± 126	4.72 ± 0.61	0.04 ± 0.06	0.74 ± 0.43	no	UVES	239
HD 5583	4986 ± 35	2.87 ± 0.09^a	-0.35 ± 0.03	1.62 ± 0.04	no	FIES	933
HD 81688	4903 ± 21	2.70 ± 0.05^a	-0.21 ± 0.02	1.54 ± 0.02	no	[b]	1350, 860
HD 82886	5123 ± 18	3.30 ± 0.04^a	-0.25 ± 0.01	1.16 ± 0.02	no	[c]	1198,1294
HD 87883	4917 ± 68	4.53 ± 0.19	0.02 ± 0.03	0.46 ± 0.21	no	ESPaDOnS	753
HIP 107773	4957 ± 49	2.83 ± 0.09^a	0.04 ± 0.04	1.49 ± 0.05	no	UVES	218
HIP 11915	5770 ± 14	4.33 ± 0.03	-0.06 ± 0.01	0.95 ± 0.02	no	HARPS	709
HIP 116454	5042 ± 72	4.69 ± 0.15	-0.16 ± 0.03	0.71 ± 0.17	no	UVES	412
HR 228	5042 ± 42	3.30 ± 0.09^a	0.07 ± 0.03	1.14 ± 0.04	no	UVES	400
KELT-6	6246 ± 88	4.22 ± 0.09^a	-0.22 ± 0.06	1.66 ± 0.13	no	FIES	374
Kepler-37	5378 ± 53	4.47 ± 0.12	-0.23 ± 0.04	0.58 ± 0.13	no	FIES	205
Kepler-444	5111 ± 43	4.50 ± 0.13	-0.51 ± 0.03	0.37 ± 0.15	no	FIES	675
mu Leo	4605 ± 94	2.61 ± 0.26^a	0.25 ± 0.06	1.64 ± 0.11	no	ESPaDOnS	354
ome Ser	4928 ± 35	2.69 ± 0.06^a	-0.11 ± 0.03	1.55 ± 0.04	no	FIES	1168
omi UMa	5499 ± 52	3.36 ± 0.07^a	-0.01 ± 0.05	1.98 ± 0.06	no	ESPaDOnS	527
Qatar-2	4637 ± 316	4.53 ± 0.62	0.09 ± 0.17	0.63 ± 0.83	no	UVES	97
SAND364	4457 ± 104	2.26 ± 0.20^a	-0.04 ± 0.06	1.60 ± 0.11	no	UVES	220
TYC+1422-614-1	4908 ± 41	2.90 ± 0.12^a	-0.07 ± 0.03	1.57 ± 0.05	no	FIES	506
WASP-37	5917 ± 72	4.25 ± 0.15	-0.23 ± 0.05	0.59 ± 0.13	no	FIES	232
WASP-44	5612 ± 80	4.39 ± 0.30	0.17 ± 0.06	1.32 ± 0.13	no	UVES	125
WASP-52	5197 ± 83	4.55 ± 0.30	0.15 ± 0.05	1.16 ± 0.14	no	UVES	125
WASP-58	6039 ± 55	4.23 ± 0.10	-0.09 ± 0.04	1.12 ± 0.08	no	FIES	310
WASP-61	6265 ± 168	4.21 ± 0.21^a	-0.38 ± 0.11	1.44 ± 0.02	yes	UVES	163
WASP-72	6570 ± 85	4.25 ± 0.13	0.15 ± 0.06	2.30 ± 0.15	no	UVES	174
WASP-73	6203 ± 32	4.16 ± 0.06^a	0.20 ± 0.02	1.66 ± 0.04	np	[d]	193,231
WASP-75	6203 ± 46	4.42 ± 0.22^a	0.24 ± 0.03	1.45 ± 0.06	no	UVES	189
WASP-76	6347 ± 52	4.29 ± 0.08^a	0.36 ± 0.04	1.73 ± 0.06	no	UVES	165
WASP-82	6563 ± 55	4.29 ± 0.10^a	0.18 ± 0.04	1.93 ± 0.08	no	UVES	239
WASP-88	6450 ± 61	4.24 ± 0.06^a	0.03 ± 0.04	1.79 ± 0.09	no	UVES	174
WASP-94 A	6259 ± 34	4.34 ± 0.07^a	0.35 ± 0.03	1.50 ± 0.04	no	UVES	356
WASP-94 B	6137 ± 21	4.42 ± 0.05^a	0.33 ± 0.02	1.29 ± 0.03	no	UVES	397
WASP-95	5799 ± 31	4.29 ± 0.05^a	0.22 ± 0.03	1.18 ± 0.04	no	UVES	247
WASP-97	5723 ± 52	4.24 ± 0.07	0.31 ± 0.04	1.03 ± 0.08	no	UVES	219
WASP-99	6324 ± 89	4.34 ± 0.12	0.27 ± 0.06	1.83 ± 0.12	no	UVES	249
WASP-100	6853 ± 209	4.15 ± 0.26^a	-0.30 ± 0.12	1.87 ± 0.02	yes	UVES	166

Notes. [(a)] Spectroscopic log g.
[(b)] Weighted average of ESPaDoNS and FIES results. The parameters are (FIES in parantheses): T_{eff} = 4870(4934) ± 30(29), log g = 2.50(2.73) ± 0.14(0.05), [Fe /H] = −0.26(−0.19) ± 0.03(0.02), and ξ_{micro} = 1.50(1.59) ± 0.03(0.03).
[(c)] Weighted average of ESPaDoNS and FIES results. The parameters are (FIES in parantheses): T_{eff} = 5124(5121) ± 22(29), log g = 3.30(3.31) ± 0.05(0.07), [Fe /H] = −0.25(−0.24) ± 0.02(0.02), and ξ_{micro} = 1.15(1.17) ± 0.03(0.04).
[(d)] Weighted average of UVES and FEROS results. The parameters are (FEROS in parantheses): T_{eff} = 6313(6162) ± 61(37), log g = 4.26(4.14) ± 0.15(0.06), [Fe /H] = 0.22(0.19) ± 0.04(0.03), and ξ_{micro} = 1.85(1.61) ± 0.08(0.04).

Table A.2. Previous parameters from SWEET-Cat.

Star	T_{eff} (K)	log g (dex)	[Fe /H] (dex)	ξ_{micro} (km/s)	Reference
BD-114672	4475 ± 100	4.10 ± 0.36	−0.48 ± 0.05	0.67 ± 0.16	Moutou et al. (2015)
BD +49 828	4943 ± 30	2.85 ± 0.09	−0.19 ± 0.06	...	Niedzielski et al. (2015b)
GJ 785	5144 ± 50	4.60 ± 0.06	0.08 ± 0.03	...	Howard et al. (2011)
HATS-1	5780 ± 100	4.40 ± 0.08	−0.06 ± 0.12	...	Penev et al. (2013)
HATS-5	5304 ± 50	4.53 ± 0.02	0.19 ± 0.08	...	Zhou et al. (2014)
HAT-P-12	4650 ± 60	4.61 ± 0.02	−0.29 ± 0.05	...	Lee et al. (2014)
HAT-P-24	6373 ± 80	4.29 ± 0.04	−0.16 ± 0.08	...	Kipping et al. (2010)
HAT-P-39	6340 ± 100	4.16 ± 0.03	0.19 ± 0.10	...	Hartman et al. (2012)
HAT-P-46	6120 ± 100	4.25 ± 0.11	0.30 ± 0.10	0.85 ± ...	Hartman et al. (2014b)
HAT-P-42	5743 ± 50	4.14 ± 0.07	0.27 ± 0.08	...	Boisse et al. (2013)
HD 120084	4892 ± 22	2.71 ± 0.08	0.09 ± 0.05	1.31 ± 0.10	Sato et al. (2013a)
HD 192263	4906 ± 57	4.36 ± 0.17	−0.07 ± 0.02	0.78 ± 0.12	Tsantaki et al. (2013)
HD 219134	4699 ± 16	4.63 ± 0.10	0.11 ± 0.04	0.35 ± 0.19	Motalebi et al. (2015)
HD 220074	3935 ± 110	1.30 ± 0.50	−0.25 ± 0.25	1.60 ± 0.30	Lee et al. (2013)
HD 220842	5920 ± 20	4.24 ± 0.02	−0.17 ± 0.02	...	Hébrard et al. (2016)
HD 233604	4791 ± 45	2.55 ± 0.18	−0.36 ± 0.04	...	Nowak et al. (2013)
HD 283668	4845 ± 66	4.35 ± 0.12	−0.75 ± 0.12	0.02 ± 0.30	Wilson et al. (2016)
HD 285507	4503 ± 73	4.67 ± 0.06	0.13 ± 0.01	...	Quinn et al. (2014)
HD 5583	4830 ± 45	2.53 ± 0.14	−0.50 ± 0.18	...	Niedzielski et al. (2016)
HD 81688	4753 ± 15	2.22 ± 0.05	−0.36 ± 0.02	1.43 ± 0.05	Sato et al. (2008)
HD 82886	5112 ± 44	3.40 ± 0.06	−0.31 ± 0.03	...	Johnson et al. (2011)
HD 87883	4958 ± 44	4.56 ± 0.06	0.07 ± 0.03	...	Valenti & Fischer (2005)
HIP 107773	4945 ± 100	2.60 ± 0.20	0.03 ± 0.10	...	Jones et al. (2015)
HIP 11915	5760 ± 4	4.46 ± 0.01	−0.06 ± 0.00	...	Bedell et al. (2015)
HIP 116454	5089 ± 50	4.59 ± 0.03	−0.16 ± 0.08	...	Vanderburg et al. (2015)
HR 228	4959 ± 25	3.16 ± 0.08	0.01 ± 0.04	1.12 ± 0.07	Sato et al. (2013b)
KELT-6	6102 ± 43	4.07 ± 0.06	−0.28 ± 0.04	...	Collins et al. (2014)
Kepler-37	5417 ± 70	4.57 ± 0.01	−0.32 ± 0.07	...	Barclay et al. (2013)
Kepler-444	5046 ± 74	4.60 ± 0.06	−0.55 ± 0.07	...	Campante et al. (2015)
mu Leo	4538 ± 27	2.40 ± 0.10	0.36 ± 0.05	1.40 ± 0.10	Lee et al. (2014)
ome Ser	4770 ± 10	2.32 ± 0.04	−0.24 ± 0.02	1.34 ± 0.04	Sato et al. (2013a)
omi UMa	5242 ± 10	2.64 ± 0.03	−0.09 ± 0.02	1.51 ± 0.07	Sato et al. (2012)
Qatar-2	4645 ± 50	4.60 ± 0.02	−0.02 ± 0.08	...	Bryan et al. (2012)
SAND364	4284 ± 9	2.20 ± 0.06	−0.02 ± 0.04	...	Brucalassi et al. (2014)
TYC+1422-614-1	4806 ± 45	2.85 ± 0.18	−0.20 ± 0.08	...	Niedzielski et al. (2015a)
WASP-37	5940 ± 55	4.39 ± 0.02	−0.40 ± 0.12	...	Simpson et al. (2011)
WASP-44	5400 ± 150	4.48 ± 0.07	0.06 ± 0.10	...	Anderson et al. (2012)
WASP-52	5000 ± 100	4.58 ± 0.01	0.03 ± 0.12	...	Hébrard et al. (2013)
WASP-58	5800 ± 150	4.27 ± 0.09	−0.45 ± 0.09	...	Hébrard et al. (2013)
WASP-61	6250 ± 150	4.26 ± 0.01	−0.10 ± 0.12	...	Hellier et al. (2012)
WASP-72	6250 ± 100	4.08 ± 0.13	−0.06 ± 0.09	1.60 ± 0.10	Gillon et al. (2013)
WASP-73	6030 ± 120	3.92 ± 0.08	0.14 ± 0.14	1.10 ± 0.20	Delrez et al. (2014)
WASP-75	6100 ± 100	4.50 ± 0.10	0.07 ± 0.09	1.30 ± 0.10	Gómez Maqueo Chew et al. (2013)
WASP-76	6250 ± 100	4.13 ± 0.02	0.23 ± 0.10	1.40 ± 0.10	West et al. (2016)
WASP-82	6490 ± 100	3.97 ± 0.02	0.12 ± 0.11	1.50 ± 0.10	West et al. (2016)
WASP-88	6430 ± 130	4.03 ± 0.09	−0.08 ± 0.12	1.40 ± 0.10	Delrez et al. (2014)
WASP-94 A	6170 ± 80	4.27 ± 0.07	0.26 ± 0.15	...	Neveu-VanMalle et al. (2014)
WASP-94 B	6040 ± 90	4.26 ± 0.06	0.23 ± 0.14	...	Neveu-VanMalle et al. (2014)
WASP-95	5630 ± 130	4.38 ± 0.03	0.14 ± 0.16	...	Hellier et al. (2014)
WASP-97	5640 ± 100	4.43 ± 0.03	0.23 ± 0.11	...	Hellier et al. (2014)
WASP-99	6180 ± 100	4.12 ± 0.03	0.21 ± 0.15	...	Hellier et al. (2014)
WASP-100	6900 ± 120	4.04 ± 0.11	−0.03 ± 0.10	...	Hellier et al. (2014)